Journal of Thermal Analysis and Calorimetry
https://doi.org/10.1007/s10973-020-09305-7

Crystallization kinetics of gehlenite glass microspheres

Melinda Majerová[1] · Anna Prnová[2,3] · Alfonz Plško[3] · Peter Švančárek[2,3] · Jana Valúchová[2,3] · Róbert Klement[3] · Dušan Galusek[2,3]

Received: 9 August 2019 / Accepted: 9 January 2020

Abstract
The glass of gehlenite composition was prepared by flame synthesis in the form of microspheres. The powder precursor was synthesised by standard solid-state reaction method using SiO_2, Al_2O_3 and $CaCO_3$. The prepared glasses were characterized from the point of view of surface morphology, phase composition and thermal properties by optical microscopy, scanning electron microscopy (SEM), X-ray diffraction (XRD) and differential scanning calorimetry (DSC), respectively. The prepared samples contained only completely re-melted spherical particles. SEM did not reveal any features indicating the presence of crystalline phases. However, traces of crystalline gehlenite were detected by XRD. The high-temperature XRD measurements (HT XRD) were carried out to identify the phase evolution during glass crystallization. In the studied temperature range, gehlenite phase was identified as the main crystalline phase. Non-isothermal DSC analysis of prepared glass microspheres was carried out from room temperature up to 1200 °C at five different heating rates: 2, 4, 6, 8 and 10 °C/min to determine the thermal properties of microspheres. In order to study the crystallization kinetics, the DSC curves were transformed into dependence of fractional extent of crystallization (α) on temperature. The Johnson–Mehl–Avrami–Kolmogorov model was found to be suitable for description of crystallization kinetics. Frequency factor $A = 5.56 \times 10^{29} \pm 1.73 \times 10^{29}$ min^{-1}, apparent activation energy $E_{app} = 722 \pm 3$ kJ mol^{-1} and the Avrami coefficient $m = 2$ were determined. In the studied system, the linear temperature dependence of nucleation rate, diffusion controlled crystal growth interface and a 2D crystal growth were confirmed.

Keywords Gehlenite · Solid-state reaction · Flame synthesis · Glass microspheres · Crystallization kinetics

Introduction

Gehlenite ($Ca_2Al_2SiO_7$) is a sorosilicate from the family of melilites, which are a large family of tetragonal, non-centrosymmetric materials. $Ca_2Al_2SiO_7$ crystallizes in the tetragonal crystal system with a space group $P\bar{4}2_1$ m, and the lattice parameters of the unit cell were $a = b = 7.868$ Å, $c = 5.068$ Å and $V = 299.390$ Å^3. In the structure of the gehlenite, the Al^{3+}, Si^{4+} and Ca^{2+} cations are localized at three types of sites: Al^{3+} ions fully occupy a regular tetrahedral site (T_1), Si^{4+} and Al^{3+} ions are statistically distributed in very distorted tetrahedral site (T_2) and Ca^{2+} ions occupy a voluminous eightfold coordinated sites called Thomson cube (TC) between the tetrahedral sheets (Fig. 1) [1–3].

Gehlenite is used as a constituent of building ceramic materials and cookware. Glass of gehlenite composition can be used in preparation of bio-soluble glass fibres and glass ceramics. From this point of view, a thorough study of the rheology of melts and crystallization of crystalline gehlenite from glass is very important [5]. Due to its structure, gehlenite can be used as a host matrix for lanthanides or transition metals. $Ca_2Al_2SiO_7$ doped with rare-earth ions has been intensively investigated over the last few decades. Doped with Nd^{3+} ions, gehlenite exhibits a wide and intensive absorption band of about 805 nm, making it a good candidate for diode pumped laser materials [6]. Ce^{3+}-doped gehlenite has long-lasting phosphoresce and can be used

✉ Melinda Majerová
melinda.majerova@savba.sk

[1] Department of Magnetometry, Institute of Measurement Science, Slovak Academy of Sciences, Dúbravská cesta 9, 842 19 Bratislava, Slovak Republic

[2] Vitrum Laugaricio – Joint Glass Center of The IIC SAS, TnU AD and FCHPT STU, Študentska 2, 911 50 Trenčin, Slovak Republic

[3] Centre for Functional and Surface Functionalized Glass, Alexander Dubček University of Trenčin, Študentska 2, 911 50 Trenčin, Slovak Republic

Published online: 21 January 2020

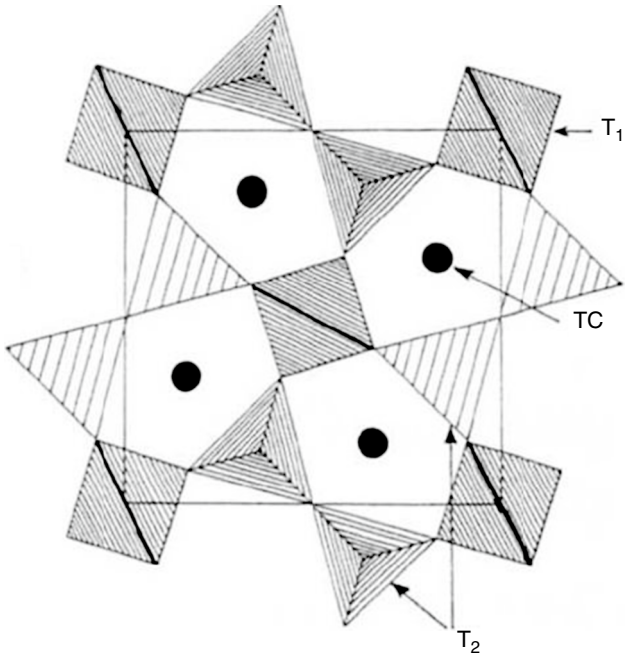

Fig. 1 Gehlenite structure; TC—Thomson cube, T_1 and T_2—regular and distorted tetrahedra [Reprinted from 4]

as tunable solid laser materials in violet and blue region [7]. The effects of the crystal field on the photoluminescent properties of $Ca_2Al_2SiO_7/Eu^{2+}$ luminophores were studied by Yang et al. [8]. They found that the photoluminescent properties of Eu^{2+} are influenced by the crystal structure of $Ca_2Al_2SiO_7$, and gehlenite thus has the potential to become a single component luminophore emitting warm white light in the production of white LEDs. Gehlenite doped with Bi^{3+} exhibits PL emissions in different spectral regions (visible, deep red and NIR range) indicating the presence of Bi in various oxidation states (Bi^{3+}, Bi^{2+} and Bi^{+}) [9].

Gehlenite glasses belong to aluminate glasses, whose preparation requires high melting temperatures and high cooling rates to avoid crystallization of the melt. Various methods are used to produce gehlenite glasses. Moesgaard and Yue used a melt-quench process [10]. The glasses were prepared in a chamber furnace by melting the mixture of SiO_2, Al_2O_3 and $CaCO_3$ in a $Pt_{90}Rh_{10}$ crucible. For the preparation of gehlenite ceramics and glass, the authors [11] used a process consisting of the heat treatment of silicone resin to which CaO and Al_2O_3 precursors in the form of nanoparticles were admixed. Shih et al. [12] used a spray pyrolysis method to prepare Eu-doped gehlenite glass particles.

Another suitable method of preparing aluminate and thus also gehlenite glasses was described by Rosenflanz et al. [13], who successfully prepare glasses with binary eutectic compositions in Al_2O_3–RE_2O_3 (RE = La, Gd and Y) and the ternary compositions Al_2O_3–RE_2O_3–ZrO_2. The glasses were prepared in the form of microspheres by flame-spraying technique: molten droplets were prepared in hydrogen–oxygen flame and quenched in water. Fully dense bulk glasses were prepared by viscous flow sintering of the microspheres in the temperature range between glass transition temperature T_g and onset of crystallization temperature T_x. Glass–ceramics materials were prepared by further heat treatment of prepared bulk glasses above T_x for a short time.

For a successful preparation of bulk gehlenite glasses from glass microspheres, a detailed knowledge of thermal properties and of the kinetics of crystallization of the prepared glass microspheres is necessary. Thermoanalytical methods, such as differential thermal analysis (DTA) and differential scanning calorimetry, are the best suited and most commonly used methods to study the thermal properties of various systems [14–20]. To get the most trusted information about phase relations, thermodynamic properties and nucleation/crystallization behaviour of prepared systems, the results of thermal analysis are usually supplemented by SEM and X-ray powder diffraction analysis [21–25].

Hou et al. [26] described the crystallization kinetics of YAG nanoparticles prepared by sonochemical sol–gel method. DSC/TG analysis was used to determine the activation energies and the Avrami constant. The results of thermal analysis were confirmed by SEM and showed that the crystallization of YAG nanoparticles proceeded simultaneously by bulk and surface crystallization, but the predominant process was the bulk crystallization.

The crystallization mechanism and properties of glass ceramics prepared from modified molten blast furnace slag by liquid–liquid mixing method were studied by Zhang et al. [27]. The main components of blast furnace slag are characterized as CaO, SiO_2 and Al_2O_3. The influence of the change in the ratio of CaO and SiO_2 on the crystallization process was monitored by DTA, XRD and field scanning electron microscope. Changing of CaO/SiO_2 ratio altered the crystallization temperature as well as the value of activation energy. Crystallization mechanism shifted from bulk to surface crystallization with increasing CaO/SiO_2 ratio. The influence of addition of Bi_2O_3 on thermal properties of melilite-based glasses and glass–ceramics was described by Reddy et al. [28]. The addition of Bi_2O_3 greatly influences the value of activation energy, E_c: it increased at the addition of 1 mass% Bi_2O_3, but further Bi_2O_3 increments significantly decreased the E_c. The crystal growth mechanism gradually changed from surface to bulk crystallization. Malecki et al. [29] studied pure and Co-, Eu-, Cr- or Th-doped gehlenite glasses prepared from $CaCO_3$, Al_2O_3, SiO_2 and Eu_2O_3 or $Co(NO_3)_3$ or $Cr(NO_3)_3$ or $Th(NO_3)_4$. The glasses were prepared in the form of microspheres by combination of the solid-state reaction and the flame synthesis. The crystallization behaviour of prepared glasses was studied by combination of DTA and TEM (Transmission electron microscopy). Co^{2+}, Th^{4+} and Eu^{3+} acted as nucleating agents and

catalysed the crystallization process. In of the Cr^{3+}-doped gehlenite glass, the activation energy of crystallization increased, due to substitution of Cr^{3+} for Al^{3+} in the glass matrix. The Johnson–Mehl–Avrami–Kolgomorov (JMAK) model was found to be suitable for description of the kinetics of crystallization of aluminate glasses [30]. Using the JMAK model, Prnova et al. [30, 31] described the crystallization kinetics of La_2O_3–Al_2O_3 and yttrium aluminate glasses.

The aim of this work is to study the crystallization kinetics of glass microspheres with gehlenite composition (50 mol% calcium oxide, 25 mol% aluminium oxide and 25 mol% silicon dioxide), prepared by combination of solid-state reaction and flame synthesis. The prepared glass microspheres were characterized by OM, SEM and XRD. HT XRD experiments were also performed to confirm the presence and crystallization of gehlenite phase. Non-isothermal DSC measurements were used for evaluation of the mechanism of crystallization. According to IUPAC recommendations [32, part 7–Model fitting methods], the Johnson–Mehl–Avrami–Kolgomorov rate Eq. (1), under non-isothermal conditions, with constant heating rate (β) was used:

$$\beta \cdot \frac{\mathrm{d}\alpha}{\mathrm{d}T} = A \cdot \exp\left[-\frac{E_{\mathrm{app}}}{RT}\right] \cdot m \cdot (1-\alpha) \cdot [-\ln(1-\alpha)]^{\left(1-\frac{1}{m}\right)}, \tag{1}$$

where α is the fractional extent of crystallization, A is pre-exponential constant of crystallization and E_{app} is the apparent activation energy of crystallization and m is strictly equal to 0.5, 1, 1.5, 2, 2.5, 3 or 4. [33–35]. The $\alpha(T)$ and $\mathrm{d}\alpha(T)/\mathrm{d}T$ values were obtained from DSC records as proportional to the area under the DSC curve after subtracting the linear baseline. For each, m was calculated E_{app} and A. For the selection of the most suitable model were used adjusted correlation coefficient (Eq. 2), Akaike information criterion (Eq. 3) and the Akaike weight (Eq. 4) [32, 36–40]:

$$R^2_{\mathrm{adj}} = 1 - \frac{\mathrm{RSS}/(n-p-1)}{\left(\sum (y_{\mathrm{i}} - \bar{y})^2\right)/(n-1)}, \tag{2}$$

$$\mathrm{AIC} = n \ln\left(\mathrm{RSS}/n\right) + 2p, \tag{3}$$

$$w\mathrm{AIC}_{\mathrm{i}} = \frac{\exp\left(-\Delta_{\mathrm{i}}/2\right)}{\sum_{\mathrm{i}=1}^{U} \exp\left(-\Delta_{\mathrm{i}}/2\right)}, \quad \text{with } 0 \le w_{\mathrm{i}} \le 1 \tag{4}$$

where y_{i}, $i = 1 \ldots n$, are data values, $\bar{y}$ is a mean of data values, RSS is residual sum of square for a model, p is the number of free parameters and $\Delta_{\mathrm{i}} = \mathrm{AIC}_{\mathrm{i}} - \mathrm{AIC}_{\mathrm{min}}$ ($\mathrm{AIC}_{\mathrm{i}}$ is the AIC values of each model, $\mathrm{AIC}_{\mathrm{min}}$ is the AIC value of the "best" model), U is the total number of models under investigation. Finally, the prevailing crystallization conditions were determined based on the value of parameter m.

Preparation of glass microspheres

The precursor powder with gehlenite composition (50 mol% calcium oxide, 25 mol% aluminium oxide and 25 mol% silicon dioxide) was prepared by solid-state reaction, from high-purity chemicals (SiO_2; p.a., Polske odczynniki chemiczne, Gliwice; Al_2O_3; p.a., Centralchem, Bratislava; $CaCO_3$ (p.a., Centralchem, Bratislava). The details are described in our previous work [9]. From precursor powder, the glass microspheres were prepared by flame synthesis [41, 42].

Characterization

The morphology and microstructure of the prepared glass microspheres were examined by optical microscopy (OM) and a scanning electron microscopy (SEM). Nikon ECLIPSE, ME 600 optical microscopy was used to observe the glass microspheres in reflected light at 10–50× magnification, to determine whether the powder precursor has completely melted in the flame and whether optically transparent particles have formed. A more detailed analysis of the microstructure of the glass microspheres was performed by SEM. Sample preparation was carried out in two ways: (1) The prepared glass microspheres were fixed to the aluminium sample holder using a conductive adhesive graphite tape. To ensure the discharge of electrical charge from the surface, they were subsequently coated with gold (Carl-Zeiss type SC-7620). (2) The microspheres were cast and pressed into a conductive phenolic resin (PhenoCure Resin Powder black). After pressing, the surface of the samples was carefully polished (Buehler Ecomet 300) to prepare cross sections of microspheres which were subsequently sputtered with carbon (JEOL JFC-1300 "AUTO Sputter Coater"). The analysis was performed by scanning electron microscope JEOL JSM-7600 F/EDS/WDS/EBSD at the accelerating voltage 20 kV. X-ray powder diffraction analysis (Panalytical Empyrean diffractometer) was used to determine the phase composition of prepared microspheres after flame synthesis and of the crystallized microspheres. High-temperature powder diffraction analysis was used to determine phase transitions during sample heating. The measurements were performed in a high-temperature diffraction cell (Anton Paar, HTK16) using the same diffractometer as above. The measurements were performed in the 2θ range of 20–55°. The temperature regime for high-temperature X-ray recording was as follows: the sample was first heated from room temperature to 600 °C at a heating rate of 10 °C min^{-1}, from 600 °C to 1100 °C, the sample was heated at a

heating rate 5 °C min^{-1} and diffraction data were recorded every 10 °C under isothermal conditions. Two long scans at 25 °C in the 2θ range 10–80° were measured at the beginning and at the end of the experiment. Diffraction data were evaluated using the software HighScore Plus (version 3.0.4, PAN Analytical, the Netherlands) with the use of the Crystalographic Open Database (COD). The DSC measurements were carried out at five heating rates (2, 4, 6, 8, 10 °C min^{-1}) in a temperature range of 30–1200 °C in nitrogen atmosphere using a simultaneous Netzsch STA 449 F1 Jupiter TG/DTA/DSC thermal analyser. The Netzsch Proteus Thermal Analysis Version 6.0.0 program was used to evaluate the measured DSC records.

Results and discussion

Morphology and phase analysis

Spherical and fully re-melted particles transparent in the visible spectrum were prepared by flame synthesis (Fig. 2a). SEM images revealed smooth surfaces of prepared microspheres and no features (e.g. angular facets) indicating the presence of crystalline phases (Fig. 2b). The absence of signs indicating the presence of crystalline phases was also confirmed by the analysis of the polished cross section of glass microspheres (Fig. 2c).

However, the X-ray diffraction pattern of the prepared microspheres (Fig. 3a) indicates the presence of low-intensity diffractions of crystalline gehlenite phase superimposed on a largely amorphous background represented by a broad-band in the range between 24° and 36°. X-ray diffraction patterns of microspheres crystallized at 1000 °C for 10 h confirmed their polycrystalline nature, with the presence of gehlenite (01-074-167 COD) as the main crystalline phase (Fig. 3b).

HT XRD analysis

The presence of gehlenite as the only crystalline phase in the whole studied temperature range 600–1100 °C was confirmed by the results of high-temperature X-ray powder diffraction analysis (Fig. 4). In HT XRD records, a shift of diffraction maxima to lower 2θ values with increasing temperature caused by the change in lattice parameters due to thermal expansion. The temperature dependence of the integral intensity of the most intensive diffraction peak corresponding to gehlenite (2θ = 31.394°; d = 2.84720 Å; [h k l] = [2 1 1]) was determined (Fig. 5) in order to quantify

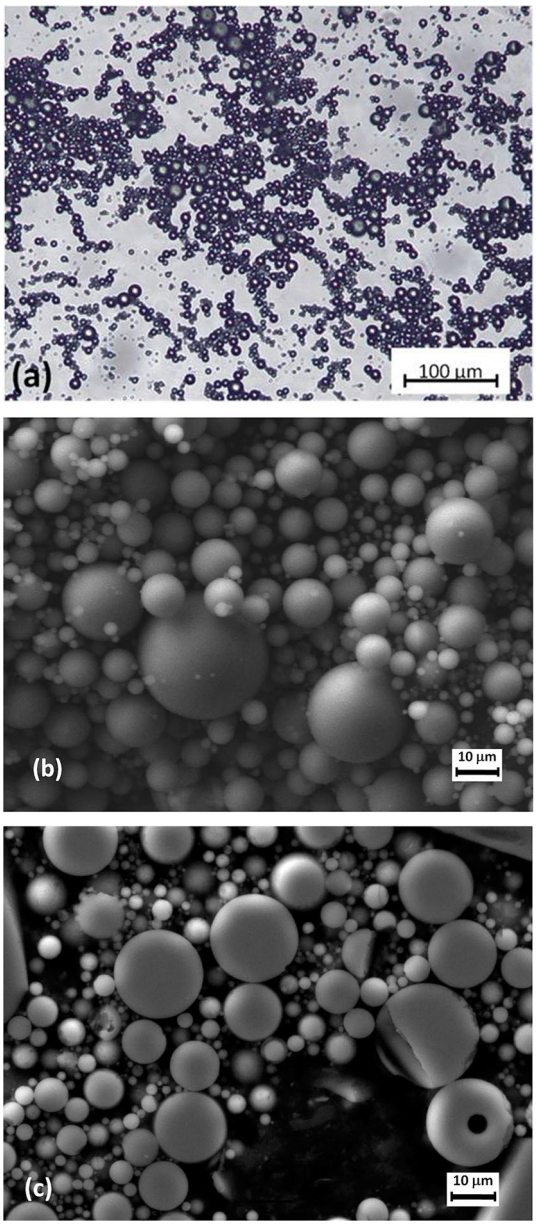

Fig. 2 The results of OM and SEM examination of prepared gehlenite microspheres. **a** OM photographs of microspheres, **b** SEM image of gehlenite microspheres, **c** SEM micrographs of a polished cross section of the gehlenite microspheres

the phase evolution in the studied temperature range. The integral intensities were normalized with respect to integral intensity of the gehlenite [h k l] = [2 1 1] diffraction maximum recorded after the whole heating cycle after cooling down to room temperature, where we could reasonably assume the sample was 100% crystalline. The onset

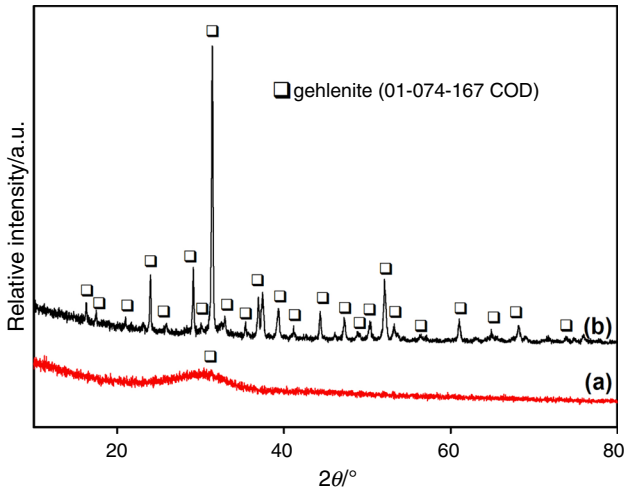

Fig. 3 X-ray powder diffraction patterns of as-prepared glass microspheres (**a**) and of the crystallized gehlenite microspheres (1000 °C/10 h) (**b**)

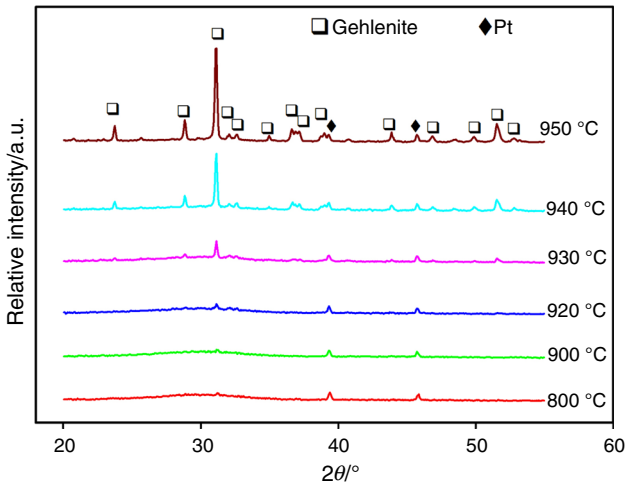

Fig. 4 HT XRD patterns of the prepared gehlenite glass microspheres recorded at various temperatures

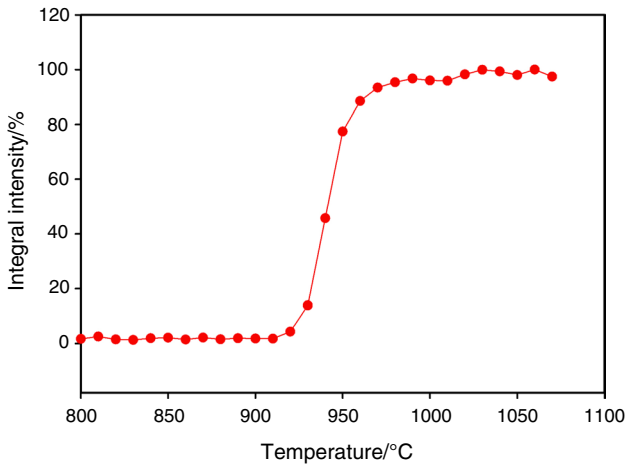

Fig. 5 Temperatures dependence of integral intensities of the [1 2 1] gehlenite diffraction peak

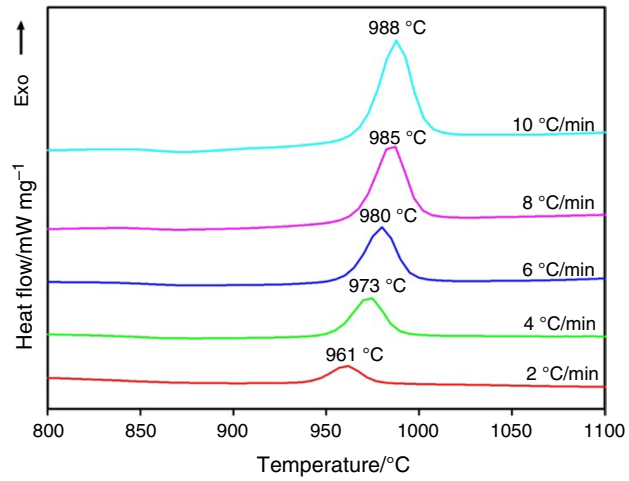

Fig. 6 DSC records of prepared gehlenite glass microspheres, recorded at the heating rates 2, 4, 6, 8 and 10 °C min^{-1}

of gehlenite phase crystallization was identified at around 910 °C. The most significant increase in the amount of crystalline phase occurs in the temperature range from 930 to 950 °C, demonstrating very fast crystallization of gehlenite from glass. Sample was fully crystalline above 970 °C. Only a negligible increase in the relative intensity of this diffraction peak was observed above this temperature.

DSC analysis

The thermal properties of gehlenite glass microspheres were examined by DSC analysis in the temperature range 30–1200 °C. Figure 9 shows the DSC records obtained at different heating rates and the corresponding values of T_p. One exothermic effect was observed on the DSC records (Fig. 6). A significant effect of the heating rate on the peak height and peak area was observed, while maximum of the peak shifted to higher temperatures with increasing heating rate (961 °C at 2 °C min^{-1} and 988 °C at 10 °C min^{-1}). From the DSC curve recorded at 10 °C min^{-1}, the glass transition temperature $T_g = 860$ °C, the crystallization onset temperature $T_x = 970$ °C and the maximum of crystallization peak temperature $T_p = 988$ °C were estimated. From the first derivative of the DSC record, the inflection points of the exothermic peak were determined ($T_{f1} = 980$ °C and $T_{f2} = 996$ °C). Based on the results of HT XRD, where we only observed the

crystallization of gehlenite in this temperature interval, the recorded exothermic peak was attributed to crystallization of gehlenite. The lower values of temperature for formation of gehlenite from HT XRD can be the result of slower heating rate (5 °C min^{-1}) and isothermal condition during records of diffraction patterns. This is also indicated by the results of the DSC analysis measured at various heating rates (Fig. 6). The results are in a good agreement with the work of Marotta et al. [43] who observed crystallization of gehlenite at about 1010 °C at heating rate 20 °C min^{-1}.

Crystallization kinetics

The values of RSS, R^2_{adj}, AIC and *w*AIC have been used to select the model which best describes the experimental data. According to the RSS and AIC criteria, the best model is the one, which assumes the minimal value. In terms of R^2_{adj} criterion, the best model is one that has the maximum value of this criterion. The main selection criterion is *w*AIC criterion, which allows by comparison the selection of the best model from model sets. If *w*AIC = 1, it means that the model is the best for describing experimental data. The values of RSS, R^2_{adj}, AIC and *w*AIC criterion for each model are summarized in Table 1. According to the values, RSS, R^2_{adj}, AIC and *w*AIC criterion, the most suitable model is the model with $m = 2$. The kinetic parameters of the crystallization process of gehlenite microspheres are as follows: frequency factor $A = 5.56 \times 10^{29} \pm 1.73 \times 10^{29}$ min^{-1}, apparent activation energy of crystallization $E_{app} = 722 \pm 3$ kJ mol^{-1} and JMAK equation with the coefficient $m = 2$. Similar value of activation energy (700 or 740 kJ mol^{-1}) was published Malecki et al. [29, 44] for pure gehlenite glass. The comparison of measured and calculated data for the model with $m = 2$ is shown in Fig. 7.

By comparing the value of Avrami parameter *m* for the studied sample in terms of works [34, 35, 45], it can be concluded with high probability that the predominant crystallization process in the gehlenite glass is controlled by diffusion with constant rate of homogeneus nucleation. The crystal growth is two-dimensional.

Table 1 Values of RSS, R^2_{adj}, AIC and *w*AIC criterions calculated for individual models with $m = 0.5$, 1, 1.5, 2, 2.5, 3 and 4

m	RSS	R^2_{adj}	AIC	wAIC
1	5.05	0.79	−5156	0
1.5	0.46	0.98	−7514	1.04×10^{-204}
2	0.17	0.99	−8453	1
2.5	0.73	0.97	−7048	8.35×10^{-306}
3	1.38	0.94	−6427	0
4	2.47	0.90	−5859	0

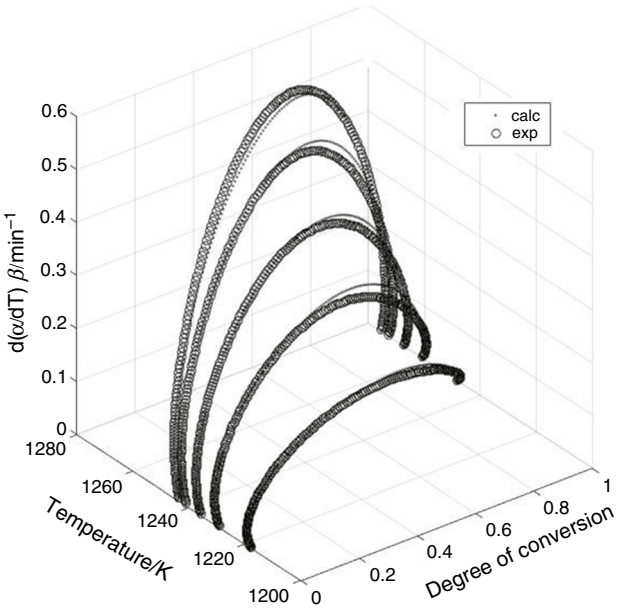

Fig. 7 Comparison of measured and calculated data for the JMAK model with $m = 2$

Conclusions

The gehlenite glass microspheres were prepared by combination of solid-state reaction and flame synthesis. The prepared glass particles were transparent and spherical. X-ray diffraction analysis revealed a small fraction of crystalline gehlenite in the glass. The DSC analysis revealed the presence of a single sharp crystallization peak, with the onset at 970 °C (measured at 10 °C min^{-1}), representing crystallization of gehlenite phase. HT XRD records confirmed the formation of only crystalline gehlenite. The kinetics parameters of crystallization process of gehlenite were determined by applying the JMAK model on the DSC data measured at five different heating rates. The determined kinetic parameters are as follows: frequency factor $A = 5.56 \times 10^{29} \pm 1.73 \times 10^{29}$ min^{-1}, apparent activation energy $E_{app} = 722 \pm 3$ kJ mol^{-1} and Avrami coefficient $m = 2$. The results indicate constant rate of homogeneous nucleation, the movement of the growth front controlled by diffusion, and two-dimensional growths of the gehlenite crystals.

Acknowledgements This paper is a part of dissemination activities of project FunGlass. This project has received funding from the European Union´s Horizon 2020, research and innovation programme under Grant Agreement No 739566. The financial support of this work by the projects VEGA 1/0527/18, APVV-17-0049, VEGA 2/0026/17, VEGA 2/0164/17 is gratefully acknowledged.

References

1. Wu H, Hu Y, Ju G, Chen L, Wang X, Yang Z. Photoluminescence and thermoluminescence of Ce^{3+} and Eu^{2+} in $Ca_2Al_2SiO_7$ matrix. J Lumin. 2011;131:2441–5. https://doi.org/10.1016/j.jlumin.2011.06.024.
2. Proverbio M, Dapiaggi M, Artioli G. Thermal expansion and excess properties of akermanite-gehlenite synthetic solid solution series. Mat Sci Forum. 2004;443–444:401–6. https://doi.org/10.4028/www.scientific.net/MSF.443-444.401.
3. Yang P, et al. $Ca_2Al_2SiO_7$:Bi^{3+}, Eu^{3+}, Tb^{3+}: A potential single-phased tunable-color-emitting phosphor. J Lumin. 2013;135:206–10. https://doi.org/10.1016/j.jlumin.2012.10.015.
4. Lejus AM, Pelletier-Allard N, Pelletier R, Vivien D. Site selective spectroscopy of Nd ions in gehlenite ($Ca_2Al_2SiO_7$), a new laser material. Opt Mater. 1996;6:129–37. https://doi.org/10.1016/0925-3467(96)00041-9
5. Ptáček P, Opravil T, Šoukal F, Havlica Holešinský R. Kinetics and mechanism of formation of gehlenite, Al-Si spinel and anorthite from mixture of kaolinite and calcite. Solid State Sci. 2013;26:53–8. https://doi.org/10.1016/j.solidstatesciences.2013.09.014.
6. Viana B, Lejus AM, Saber D, Duxin N, Vivien D. Optical properties and energy transfer among Nd^{3+} in Nd:$Ca_2Al_2SiO_7$ crystals for diode puped lasers. Opt Mater. 1994;3:307–16. https://doi.org/10.1016/0925-3467(94)90043-4.
7. Kodama N, Tanii Y, Yamaga M. Optical properties of long-lasting phosphorescent crystals Ce3 + -doped Ca2Al2SiO7 and CaYAl3O7. J Lumin. 2000;87–89:1076–8. https://doi.org/10.1016/S0022-2313(99)00543-8.
8. Yang P, Yu X, Yu H, Jiang T, Zhou D, Qiu J. Effects of crystal field on photoluminescence properties of $Ca_2Al_2SiO_7$:Eu^{2+} phosphors. J Rare Earths. 2012;30:1208–12. https://doi.org/10.1016/S1002-0721(12)60207-5.
9. Majerova M, Klement R, Prnova A, Kraxner J, Bruneel E, Galusek D. Crystallization and VIS-NIR luminescence of Bi-doped gehlenite glass. R Soc Open Sci. 2018;5:181667. https://doi.org/10.1098/rsos.181667.
10. Moesgaard M, Yue Y. Compositional dependence of fragility and glass forming ability of calcium aluminosilicate melts. J Non-Cryst Solids. 2009;355:867–73. https://doi.org/10.1016/j.jnoncrysol.2009.04.004.
11. Bernardo E, Fiocco L, Prnová A, Klement R, Galusek D. Gehlenite: Eu^{3+} phosphors from a silicone resin and nano-sized fillers. Opt Mater. 2014;36:1243–9. https://doi.org/10.1016/j.optmat.2014.03.007.
12. Shih SJ, et al. Preparation and characterization of Eu-doped gehlenite glassy particles using spray pyrolysis. Ceram Int. 2016;42:11324–9. https://doi.org/10.1016/j.ceramint.2016.04.053.
13. Rosenflanz A, Frey M, Endres B, Anderson T, Richards E, Schardt C. Bulk glasses and ultrahard nanoceramics based on alumina and rare-earth oxides. Nature. 2004;430:761–4. https://doi.org/10.1038/nature02729.
14. Yigiter AO, Atakol MK, Aksu ML, Atakol O. Thermal characterization and theoretical and experimental comparison of poryl chloride derivatives of heterocyclic energetic compounds. J Therm Anal Calorim. 2017;127:2199–213. https://doi.org/10.1007/s10973-016-5766-2.
15. Pawlikowska M, Piatkowska M, Tomaszewicz E. Synthesis and thermal stability of rare-earths molybdates and tungstates with fluorite- and scheelite-type structure. J Therm Anal Calorim. 2017;130:69–76. https://doi.org/10.1007/s10973-017-6127-5.
16. Rahvard MM, Tamizifar M, Boutorabi SM. Non-isothermal crystallization kinetics and fragility of $Zr_{56}Co_{28}Al_{16}$ and $Zr_{56}Co_{22}Cu_6Al_{16}$ bulk metallic glasses. J Therm Anal Calorim. 2018;134:903–14. https://doi.org/10.1007/s10973-018-7367-8.
17. Kalenda P, Koudelka L, Mošner P, Beneš L, Drobná H. Thermoanalytical study and crystallization of $Ba(PO_3)_2$–WO_3 glasses. J Therm Anal Calorim. 2019;137:1911–8. https://doi.org/10.1007/s10973-019-08115-w.
18. Koga N, Kikuchi S. Thermal behavior of perlote concrete used in a sodium-cooled fast reactor. J Therm Anal Calorim. 2019;138:983–96. https://doi.org/10.1007/s10973-019-08351-0.
19. Laboureur D, Glabeke G, Gouriet JB. Aluminum nanoparticles oxidation by TGA/DSC. J Therm Anal Calorim. 2019;137:1199–210. https://doi.org/10.1007/s10973-019-08058-2.
20. Dande A, et al. DSC analysis of human synovial fluid samples in the diagnostics of non-septic and septic arthritis. J Therm Anal Calorim. 2017;130:1249–52. https://doi.org/10.1007/s10973-017-6179-6.
21. Chen J, He F, Xiao Y, Xie M, Xie J, Zhang W, Shi J. Effect of Al/Si ratio on the crystallization properties and structure of mold flux. Con Build Mat. 2019;216:19–28. https://doi.org/10.1016/j.combuildmat.2019.04.261.
22. Mukherjee DP, Das SK. SiO2–Al2O3–CaO glass-ceramics: effects of CaF2 on crystallization, microstructure and properties. Ceram Int. 2012;39:571–8. https://doi.org/10.1016/j.ceramint.2012.06.066.
23. Niculescu M, et al. Thermal and spectroscopic analysis of Co(II)-Fe(III) polyglyoxylate obtained through reaction of etylene glykol with metal nitrates. J Therm Anal Calorim. 2018;131:127–36. https://doi.org/10.1007/s10973-016-6079-1.
24. Lu J, Li Y, Zou Ch, Liu Z, Wang C. Effect of heating rate on the sinterability, crystallization, and mechanical properties of sintered glass-ceramics from granite waste. J Therm Anal Calorim. 2019;135:1977–85. https://doi.org/10.1007/s10973-018-7346-0.
25. Prnova A, et al. Thermal behavior of yttrium aluminate glasses studied by DSC, high-temperature X-ray diffraction, SEM and SEM-EDS. J Therm Anal Calorim. 2017;128(3):1407–15. https://doi.org/10.1007/s10973-016-6078-2.
26. Hou JG, Kumar RV, Qu YF, Krsmanovic D. Crystallization kinetics and densification of YAG nanoparticles from various chelating agents. Mater Res Bull. 2009;44:1786–91. https://doi.org/10.1016/j.materresbull.2009.03.001.
27. Zhang W, He F, Xie J, Liu X, Fang D, Yang H, Luo Z. Crystallization mechanism and properties of glass ceramics from modified molten blast furnace slag. J Non-Cryst Solids. 2018;502:164–71. https://doi.org/10.1016/j.jnoncrysol.2018.08.024.
28. Reddy AA, et al. Study of melilite based glasses and glass-ceramics nucleated by Bi_2O_3 for functional applications. RSC Adv. 2012;2(29):10955–67. https://doi.org/10.1039/C2RA22001F.
29. Malecki A, Gajerski R, Labus S, Prochovska-Klisch B, Oblakowski J. Kinetics and mechanism of crystallization of gehlenite glass pure and doped with Co^{2+}, Eu^{3+}, Cr^{3+} and Th^{4+}. J Non-Cryst Solids. 1997;212:55–8. https://doi.org/10.1016/S0022-3093(96)00537-6.
30. Prnova A, Plsko A, Valuchova J, Svancarek P, Klement R, Michalkova M, Galusek D. Crystallization kinetics of yttrium aluminate glasses. J Therm Anal Calorim. 2018;133(1):227–36. https://doi.org/10.1007/s10973-017-6948-2.

31. Prnova A, et al. Crystallization kinetics of binary La_2O_3–Al_2O_3 glass. J Non-Cryst Solids. 2018;501:55–61. https://doi.org/10.1016/j.jnoncrysol.2018.03.001.
32. Vyazovkin S, et al. ICTAC Kinetics Committee recommendations for performing kinetic computations on thermal analysis data. Thermochim Acta. 2011;520:1–19. https://doi.org/10.1016/j.tca.2011.03.034.
33. Johnson WA, Mehl RF, Mehl RF. Reaction kinetics in processes of nucleation and growth. Trans Am Inst Min Metall Pet Eng. 1939;135:416–42.
34. Šesták J, Šimon P. Thermal analysis of micro, nano- and non-crystalline materials: transformation, crystallization, kinetics and thermodynamics. Netherlands: Springer; 2013.
35. Tanaka H. Thermal analysis and kinetics of solid state reaction. Thermochim Acta. 1995;267:29–44. https://doi.org/10.1016/0040-6031(95)02464-6.
36. Johnson JB, Omland KS. Model selection in ecology and evolution. Trends Ecol Evol. 2004;19:101–8. https://doi.org/10.1016/j.tree.2003.10.013.
37. Akaike H. A new look at the statistical model identification. IEEE Trans Autom Control. 1974;19:716–23. https://doi.org/10.1109/TAC.1974.1100705.
38. Málek J. The applicability of Johnson-Mehl-Avrami model in the thermal analysis of the crystallization kinetics of glasses. Thermochim Acta. 1995;267:61–73. https://doi.org/10.1016/0040-6031(95)02466-2.
39. Cavanaugh JE. Criteria for linear model selection based on Kullback's symmetric divergence. Aust N Y Stat. 2004;46:257–74. https://doi.org/10.1111/j.1467-842X.2004.00328.x.
40. Kim HJ, Cavanaugh JE. Model selection criteria based on Kullback information measures for nonlinear regression. J Stat Plan Inference. 2005;134:332–49. https://doi.org/10.1016/j.jspi.2004.05.002.
41. Haladejova K, Prnova A, Klement R, Tuanb WH, Shihc SJ, Galusek D. Aluminate glass based phosphors for LED applications. J Eur Ceram Soc. 2016;36:2969–73. https://doi.org/10.1016/j.jeurceramsoc.2015.11.027.
42. Klement R, Hruska B, Hronsky V, Olcak D. Preparation and characterization of basic and Er^{3+} doped glasses in the system Y_2O_3–Al_2O_3–ZrO_2. Acta Phys Pol A. 2014;126:302–3. https://doi.org/10.12693/APhysPolA.126.302.
43. Marotta A, Buri A, Valenti GL. Crystallization kinetics of gehlenite glasses. J Mat Sci. 1978;13:2483–6.
44. Malecki A, Lejus AM, Viana B, Vivien D, Collongues R. Spectroscopic studies of the kinetics of devitrification of Nd^{3+}-doped glasses in the akermanite-gehlenite system. J Non-Cryst Solids. 1994;170:161–6. https://doi.org/10.1016/0022-3093(94)90042-6.
45. Šesták J, Šatava V, Wendlandt WW. The study of heterogeneous processes by thermal analysis. Thermochim Acta. 1973;7:333–556. https://doi.org/10.1016/0040-6031(73)87019-4.